Published in final edited form as:
Dalton Trans. 2011 June 21; 40(23): 6226–6237. doi:10.1039/c0dt01618g.

Biocompatible inorganic nanoparticles for [^{18}F]-fluoride binding with applications in PET imaging

Maite Jauregui-Osoro[a], **Peter A. Williamson**[a], **Arnaud Glaria**[a], **Kavitha Sunassee**[a], **Putthiporn Charoenphun**[a], **Mark A. Green**[b], **Gregory E. D. Mullen**[a], and **Philip J. Blower**[*,a]

[a]Division of Imaging Sciences, King's College London, St. Thomas' Hospital, London, UK SE1 7EH

[b]Department of Physics, King's College London, The Strand, London, WC2R 2LS

Abstract

A wide selection of insoluble nanoparticulate metal salts was screened for avid binding of [^{18}F]-fluoride. Hydroxyapatite and aluminium hydroxide nanoparticles showed particularly avid and stable binding of [^{18}F]-fluoride in various biological media. The *in vivo* behaviour of the [^{18}F]-labelled hydroxyapatite and aluminium hydroxide particles was determined by PET-CT imaging in mice. [^{18}F]-labelled hydroxyapatite was stable in circulation and when trapped in various tissues (lung embolisation, subcutaneous and intramuscular), but accumulation in liver *via* reticuloendothelial clearance was followed by gradual degradation and release of [^{18}F]-fluoride (over a period of 4 h) which accumulated in bone. [^{18}F]-labelled aluminium hydroxide was also cleared to liver and spleen but degraded slightly even without liver uptake (subcutanenous and intramuscular). Both materials have properties that are an attractive basis for the design of molecular targeted PET imaging agents labelled with ^{18}F.

Introduction

Selective binding of fluoride ions to various solid state and soluble materials has been a topic of growing interest in recent years for applications including extraction and analysis of fluoride in environmental samples,[1-3] rapid trapping of [^{18}F]-fluoride following its manufacture in cyclotrons and in purification of [^{18}F]-labelled radiopharmaceuticals for positron emission tomography,[4] and most recently as inorganic binding sites for incorporation of [^{18}F]-fluoride into biomolecules.[5-12] Various solid state materials have been used including anion exchange resins,[4] alumina,[13,14] hydroxyapatite,[15-17] porous titania,[18] aluminosilicates,[19,20] molecular materials containing silicon,[10-12,21] boron[2,8,22] and phosphorus,[9] and complexes of aluminium[5-7] and zirconium.[3] Stimulated by the well-known strong adsorption of fluoride ions onto hydroxyapatite,[15,17,23] which occurs even *in vivo* in the face of competition from, for example, phosphate ions, phosphonates, polyphosphates (*e.g.* nucleotides) and hydroxide ions, we are interested in inorganic nanoparticulate materials that may be used as targeted carriers of [^{18}F]-fluoride ions for *in vivo* PET imaging applications.

Use of nanoparticulate and microparticulate materials for radionuclide imaging, most recently in combination with other imaging modalities (especially MRI and optical imaging), has been a topic of growing interest in recent years.[24-26] Methods for derivatisation of nanoparticles (NPs) such as superparamagnetic iron oxides (SPIO), drug-

[*]Philip.Blower@kcl.ac.uk; Tel: 0207-188-9513.

Europe PMC Funders Author Manuscripts

carrying micelles and liposomes, and quantum dots for radiolabelling have been developed, most often entailing covalent derivatisation of a silica or polymer coating on the particle surface, with prosthetic groups such as organic moieties for covalent labelling with ^{18}F[24-26] or with bifunctional chelating agents for metallic radionuclides such as ^{99m}Tc[27] and ^{64}Cu.[28] We envision a targeted inorganic nanoparticulate formulation in which the nanoparticle surface is derivatised with both a targeting moiety such as a protein or peptide, and a detectable probe such as a positron or gamma emitting radionuclide and/or a beta- or alpha-emitting therapeutic radionuclide, and in which the surface derivatisation exploits the intrinsic binding properties of the inorganic nanoparticle itself, rather than an encapsulating polymer or membrane. Our purpose here is to identify inorganic materials that have sufficient intrinsic affinity for the radiolabel that stable, direct labelling of the inorganic nanoparticle material itself can be achieved, for radionuclide imaging and therapy applications *in vivo*. Such materials would have to be biocompatible and/or biodegradable and non-toxic. Their surface chemistry should be readily amenable to derivatisation with targeting molecules such as proteins, peptides, carbohydrates and nucleic acids, and the radiolabelling step should be achievable rapidly and efficiently under mild conditions compatible with sensitive biomolecules and with the minimum of chemical manipulation. ^{18}F was chosen as an initial radionuclide because of its ubiquitous availability resulting from the widespread clinical use of [^{18}F]-fluorodeoxyglucose, and the excellent physical properties of its emissions for PET imaging (half life 110 min and high-yield low-energy positron).[29] It is by far the most readily available and widely used of the positron emitting radionuclides, and consequently the most likely to be of benefit to patients.

In this paper we describe the results of an initial survey of the [^{18}F]-fluoride binding properties of inorganic materials that were considered likely to have an affinity for fluoride. Those that showed the most promise in terms of efficacy of [^{18}F]-fluoride binding and biocompatibility were subjected to further evaluation *in vitro* to determine the affinity, capacity and stability of the interaction in biological media, and *in vivo* by PET-CT imaging in mice to determine the biodistribution and fate of the radiolabel. We included in our survey materials already known to have a degree of biocompatibility, including hydroxyapatite[16] (already used for *in vivo* applications such as bone grafting), aluminium hydroxides (used safely *in vivo* as adjuvants in vaccines),[30,31] calcium phosphate (also used as adjuvants[32]) and silica (for which derivatisation chemistry is well-established[33] and clinical trials of modified silica nanoparticles[34] have recently been approved). A list of the particulate and nanoparticulate materials used, and their origin, is provided in Table 1. Hydroxyapatite showed particular promise in preliminary studies and for this reason further hydroxyapatite nanoparticle formulations were synthesised and evaluated to determined the effect of post-synthesis treatments (calcination, hydrothermal treatment and surface derivatisation) on morphology and fluoride binding affinity. These new formulations are summarised in Table 2.

Experimental section

Synthesis of nanoparticles

All chemicals were obtained from commercial sources as analytical reagents and used without further purification unless otherwise indicated. MeO-PEG-COOH (α-methoxy-ω-carboxylic acid poly(ethylene glycol), Mw 2000) was purchased from Iris-Biotech GmbH. Calcium nitrate tetrahydrate ($Ca(NO_3)_2{\cdot}4H_2O$), ammonium phosphate dibasic ($(NH_4)_2HPO_4$), cetyltrimethylammonium bromide (CTAB, $C_{19}H_{42}NBr$), cetyltrimethylammonium chloride solution 25% in H_2O (CTAC, $C_{19}H_{42}NCl$), triethanolamine (TEA, $C_6H_{15}NO_3$) and tetraethyl orthosilicate (TEOS, $C_8H_{20}O_4Si$) were

purchased from Sigma–Aldrich. Deionised water (Type I, 18.2 MΩ·cm) was obtained from an ELGA Purelab Option-Q system.

Preparation of HA2 (calcined hydroxyapatite)—To a solution of 0.5 M $Ca(NO_3)_2{\cdot}4H_2O$ in H_2O (30 ml) was added 0.3 M $(NH_4)_2HPO_4$ in H_2O (30 ml) drop-wise. The solutions were adjusted to pH 10 with 28% ammonium hydroxide prior to mixing. The reaction mixture was stirred for 4 h at 60 °C and left to stand overnight. The precipitate was washed four times with ethanol (20 ml) with centrifugation at 8,000 rpm (7513 g) to remove the washings. The product was dried at 60 °C overnight to produce "untreated" hydroxyapatite. This material was sintered in a furnace at 550 °C for 6 h yielding a fine white powder.

Preparation of HA3 (hydrothermally treated hydroxyapatite)—"Untreated" hydroxyapatite was prepared as described above for HA2. The HA powder was then suspended in water (15 mg ml^{-1}), placed in an acid digestion bomb (Parr) and heated in an oven at 200 °C for 24 h followed by freeze drying.

Preparation of HA4 (no thermal treatment)—In a typical experiment, 20 ml aqueous solutions of $Ca(NO_3)_2{\cdot}4H_2O$ and $(NH_4)_2HPO_4$ were freshly prepared with a concentration of 0.75 M. The pH of these solutions was adjusted to 9 by addition of small amounts of a concentrated NH_4OH solution (Fluka). Then in a 50 ml double-neck rounded flask, 5.00 ml of the calcium nitrate solution were added to 5.52 ml of H_2O and 0.75 ml of a CTAB aqueous solution (0.1 M). When the temperature reached 80 °C, 2.98 ml (ratio Ca/P was thus 1.68) of the ammonium phosphate solution were added in one portion, producing a white suspension which was magnetically stirred for 2 h. The white precipitate was then collected by centrifugation at 1500 rpm (1409 g) for 5 min and washed twice with H_2O removing the washings by centrifugation, to remove CTAB. Finally the solid was washed with ethanol and dried under vacuum at 80 °C.

Functionalisation of HA4 with Alendronate (Ale) or MeO-PEG-COOH (PEG)—Alendronate (4-amino-1-hydroxy-1-phosphonobutyl phosphonic acid, monosodium) was synthesised as described in the literature.[35] Aqueous solutions of the ligands (Ale or MeO-PEG-COOH) were prepared with a concentration of 0.05 M. In the case of MeO-PEG-COOH, the solution was made in 0.1 M 2-(*N*-morpholino)ethanesulfonic acid (MES) buffer (pH 6.15) to avoid the dissolution of the NPs at lower pH. The previously synthesised NPs were suspended in water at a concentration of 10 mg ml^{-1} and 100 μl of this suspension was mixed with 100, 300 or 500 μl of the ligand solution. The final volume of the solution was adjusted to 1 ml by addition of water so that the final concentration of ligand in these mixtures was respectively 5, 15 or 25 mM. The mixture was left to react overnight under agitation, and heated for one hour at 80 °C before washing the NPs twice with water and centrifuging (1500 rpm, 1409 g, for 5 min). The resulting materials were named HA4Ale-0.1, -0.3, -0.5 and HA4PEG-0.1, -0.3, -0.5 respectively, according to the volume of ligand solution added.

Preparation of Mes-SiO_2 nanoparticles—Mesoporous silica NPs were obtained by a modification of the synthesis described by Bein *et al.*[36] Briefly 64.0 ml of deionised water was mixed with 10.5 ml of MeOH (0.259 mol), 10.4 ml of CTAC (7.8 mmol) and 12.37 ml of TEA (93 mmol). Twenty ml of this solution was stirred for 30 min at 60 °C and 1.45 ml of TEOS (6.5 mmol) was added dropwise over 3 min. The molar ratios were TEOS/CTAC/TEA/H_2O–MeOH: 1/0.24/3/109/5.5. The solution was stirred for a further 2 h before addition of 100 ml of methanol which induced precipitation of the particles. The suspension was centrifuged at 2000 rpm (1878 g) for 10 min. The pellet was washed with methanol and

dried at 60 °C under vacuum. The template molecules were then removed by washing the particles with an acidic methanol solution (21.9 ml of 5 M HCl in 100 ml of methanol) at room temperature overnight.

Characterisation of particulate materials

FT-IR studies were performed using either a Perkin–Elmer Spectrum RXI FT-IR spectrometer or a Perkin–Elmer Spectrum 100 spectrometer equipped with a Universal Attenuated Total Reflectance (UATR) sampling accessory. Transmission electron microscopy (TEM) was performed either with an FEI Tecnai T12 instrument at 120 kV or a FEI Tecnai T20 instrument with a LaB_6 filament operating at 200 kV. The samples were prepared by evaporation of a drop of the aqueous colloidal suspensions onto a carbon-coated copper grid (Agar Scientific 200 mesh). X-ray powder diffraction (XRD) was recorded on a PANalytical X'Pert Pro Multi Purpose diffractometer. Zeta potential measurements were made 25 °C using a Delsa Nano C particle analyser. Particles were suspended in water (1 mg ml^{-1}) at pH7. Dynamic light scattering (DLS) measurements were performed with a Beckman Coulter DelsaNano C instrument at 25 °C with particles suspended in water at 1 mg ml^{-1} for Alhydrogel™, HA4, HA4Ale, HA4PEG and 0.2 mg ml^{-1} for HA1, HA2 and HA3.

Initial screening for [^{18}F]-fluoride binding

[^{18}F]-fluoride was produced by irradiation of [^{18}O]-water (97 atom%, Isochem Ltd., Hook, UK) with 11 MeV protons from a CTI RDS 112 cyclotron (beam current 30 μA). This solution in [^{18}O]-water was used without further purification. The ^{18}F is nominally in the form of no-carrier-added fluoride ions, although typically ^{19}F is also present in traces. Initial studies were performed using hydroxyapatite nanoparticles, and focused on testing the optimal medium in which to carry out the radiolabelling and optimal incubation times required. [^{18}F]-fluoride solution (100 μl, 6 MBq) was added to a 1 mg ml^{-1} suspension of HA in water (1 ml), and the mixture was incubated at room temperature with continuous shaking for 5, 10, 20 and 60 min. Since labelling efficiency had plateaued by 5 min in these experiments, a standard incubation time of 5 min was adopted for screening of all materials. Each sample was then tested in triplicate, and nanoparticle-free standards were also tested in order to determine baseline supernatant activity and non-specific binding to tubes. To measure binding of radioactivity to particles, the mixture was then centrifuged (5 min at 10000 rpm, 9391 g) and an aliquot of the supernatant (100 μl) was collected from each sample. The radioactivity in this aliquot was measured using a gamma counter and expressed as the percentage of the total added to the sample. The % radioactivity associated with the nanoparticles was calculated using the following equation:

$$\text{Labeling efficiency } (\%) = [1 - (\text{activity in sample aliquot}/\text{activity in standard aliquot})] \times 100 \quad (1)$$

To check that small quantities of material (*e.g.* in quantities that might be injected *in vivo*) have sufficient capacity for efficient binding of no-carrier-added [^{18}F]-fluoride, different concentrations of nanoparticles were labelled with [^{18}F]-fluoride. For both hydroxyapatite and aluminium hydroxide, these concentrations varied between 0.025 and 1.0 mg ml^{-1}.

To provide an objective measure of fluoride binding affinity allowing semi-quantitative comparison between materials, we adopted particle concentration at half-maximal % binding after 5 min incubation of no-carrier-added [^{18}F]-fluoride with suspensions containing different concentrations of particles; this is equivalent to a dissociation constant when expressed in suitable units. The data were fitted to eqn (2), a sigmoid function from which

the maximum binding (B_{max}) and the particle concentration at half-maximal % binding (K_d) were obtained, using Solver in Microsoft Excel.

$$Y = B_{max}(X^n) / ({K_d}^n + X^n) \quad (2)$$

where X is nanoparticle concentration and Y is % bound radioactivity.

To study the fluoride loading capacity of these materials, a radiolabelling study was carried out with ^{18}F as above but in the presence of varying concentrations of *cold* (non-radioactive) sodium fluoride (X) at different particle concentrations (0.1, 0.5 and 1 mg ml^{-1}).

Competition studies

One hundred microlitres of solutions containing different concentrations of the potential competitor/inhibitor (see ESI Table S1 for full list) were added to 1 ml of a 0.5 mg ml^{-1} (unless otherwise stated) suspension of nanoparticles in water. Aqueous [^{18}F]-fluoride (100 μl) was then added to each sample and the mixture was incubated at room temperature with continuous shaking for 5 min. The samples were then centrifuged for 5 min at 10000 rpm (9391 g), and an aliquot of the supernatant (100 μl) was collected from each sample. The % bound radioactivity was determined as described above (eqn (1)).

Binding in serum—[^{18}F]-fluoride (100 μl) was added to a 0.5 mg ml^{-1} suspension of particles in human serum (Sigma Aldrich), and the mixture was incubated at 37 °C with continuous shaking for 6 h. Each sample was tested in triplicate, and standard samples without nanoparticles were also tested as a control. The mixture was centrifuged (5 min at 10000 rpm, 9391 g). Under these conditions, serum proteins do not sediment while the nanoparticles do so efficiently. Aliquots of the supernatant (100 μl) were collected from each sample at different time intervals. The % radioactivity bound to particles was determined as above (eqn (1)). To identify possible components of serum that may be responsible for the reduction or delay in fluoride binding, HA particles were incubated with human serum albumin (4 mg ml^{-1}, *cf.* typically present at 40 mg ml^{-1} in serum) and with fetuin, a protein that binds strongly to HA and is present in serum (0.1 mg ml^{-1}, *cf.* typically 0.5 mg ml^{-1} in serum).

Kinetic stability studies

Kinetic stability in water—Each sample was tested in triplicate. Aqueous [^{18}F]-fluoride (100 μl, 6 MBq) was added to a 1 mg ml^{-1} suspension (1 ml) of nanoparticles in water, and the mixture was incubated at room temperature with continuous shaking for 5 min. The mixture was centrifuged (5 min at 10000 rpm, 9391 g), the supernatant was discarded and the percent radioactivity associated with the nanoparticles was calculated using eqn (3):

$$\text{Labelling efficiency (\%)} = [(\text{Activity of nanoparticles})/(\text{input activity})] \times 100 \quad (3)$$

The particles were then resuspended in water (1 ml), and the mixture was shaken for 5 min and centrifuged. The supernatant was discarded and the % particle-bound activity measured again. This washing step was repeated 3 times.

Kinetic stability in competitive media—Each sample was tested in triplicate, and compared with standard particle-free solutions. [^{18}F]-fluoride (100 μl, 6 MBq) was added to a suspension of nanoparticles (1 mg ml^{-1}) in water (1 ml) and the mixture was incubated at room temperature with continuous shaking for 5 min. The mixture was then centrifuged (5 min at 10000 rpm, 9391 g) and an aliquot of the supernatant (100 μl) was collected from

each sample. The % bound radioactivity was determined as described above using eqn (1). The pellet was then resuspended and a 0.01 M solution of the chosen competitor/inhibitor (100 μl; see ESI Table S1 for list) was then added to each sample. Samples were then incubated at 25 °C with continuous shaking for up to 120 min. Every 30 min, the mixture was centrifuged (5 min at 10000 rpm, 9391 g) and an aliquot of the supernatant (100 μl) was collected from each sample. The % bound radioactivity was calculated as before using eqn (1).

Kinetic stability in serum—HA and aluminium hydroxide particles suspended in water (1 mg ml^{-1}) were labelled with [^{18}F]-fluoride (100 μl) as described above, in triplicate. The mixture was centrifuged (5 min at 10000 rpm, 9391 g), the supernatant was discarded and % radioactivity associated with the nanoparticles was measured as described above (eqn (3)). The pellets were then resuspended in human serum (1 ml) and incubated at 37 °C with continuous shaking for up to 40 min. At different time intervals the samples were centrifuged and the activity associated with the nanoparticles was measured, and the pellets resuspended in the serum for continued incubation.

In vitro macrophage uptake studies

Media and reagents were obtained from PAA (Yeovil, UK). The J774.1 cell line (macrophage, derived from a tumour in a female BALB/c mouse, kindly provided by Dr Helen Collins, King's College London) was grown in a humidified incubator at 37 °C with 5% CO_2 in Dulbecco's Modified Eagle Medium (DMEM) supplemented with 10% foetal calf serum (FCS), 10 mM HEPES, 1 mM sodium pyruvate, 2 mM L-glutamine and penicillin/streptomycin.

To measure uptake of [^{18}F]-labelled nanoparticles in macrophages, J774.1 cells were seeded in a 24 well plate at a density of 5×10^5 cells per well, incubated in a humidified incubator at 37 °C with 5% CO_2 for 24 h and washed twice in Hank's balanced salt solution (HBSS). Next, [^{18}F]-fluoride labelled particles in HBSS (0.5 ml of a 20 μg ml^{-1} particle suspension) were added and cells were incubated at 37 °C for up to 3 h. At different time intervals, cells were washed twice with 500 μl cold HBSS (the washings contain labelled particles and soluble radioactivity but not cells) and extracted with 500 μL 1 M NaOH (this extract contains all cell-bound radioactivity) for 10 min. The cell medium/washings and cell extracts were counted in a gamma counter (Wallac 1282-001 Compugamma CS). Percent accumulation in cells was plotted *versus* incubation time. The same experiments were carried out in a cell-free 24 well plate, and uptake into cells of soluble [^{18}F]-fluoride without particles were also studied as controls.

Phagocytic uptake of hydroxyapatite and aluminium hydroxide nanoparticles was demonstrated by transmission electron microscopy as follows. J774.1 cells were seeded in 6 well plates at a density of 5×10^5 cells per well in the above medium (2 ml) and incubated in a humidified incubator at 37 °C with 5% CO_2 for 48 h. HA1 and HA2 or $Al(OH)_3$ particles (2 ml, 100 μg ml^{-1}) in phosphate buffered saline (PBS) were added to the cells and incubated at 37 °C, 5% CO_2 for 2–4 h. Cells were washed three times with HBSS (2 ml) and detached from the wells by scraping. The cells were pelleted by centrifugation at 1500 rpm (1409 g) for 5 min and resuspended in piperazine-*N*,*N*′-bis(2-ethanesulfonic acid) buffer (PIPES) 0.1 M (1 ml). Cells were then fixed by adding 4% glutaraldehyde (1 ml) and incubating for 1 h before washing twice and resuspending in 0.1 M PIPES buffer (1 mL), post fixed in 1% aqueous osmium tetroxide and dehydrated through a graded series of ethanol and embedded in TAAB resin. Sections 70 nm thick were cut using a Leica ultracut E ultramicrotome (Leica, Milton Keynes, UK), mounted on 200 mesh Cu grids (Agar Scientific, Stansted, UK), and stained with 1.5% uranyl acetate in 50% ethanol and 0.15%

lead citrate before viewing on a Tecnai T12 electron microscope (FEI, the Netherlands). Images were captured using a Gatan Bioscan 792 camera (Gatan, Abingdon Oxon, UK).

In vivo studies

Animal studies were carried out in accordance with UK Research Councils' and Medical Research Charities' guidelines on Responsibility in the Use of Animals in Bioscience Research, under a UK Home Office licence. Female BALB/c mice (aged 7–12 weeks, 20.5 ± 3.4 g) were purchased from Harlan Laboratories, UK. For HA, mice received i.v. (tail vein) injections of approximately 5 MBq of [^{18}F]-fluoride-labelled nanoparticles (1 mg ml^{-1}), prepared as described above in 50 μl saline (Fresenius Kabi). For $Al(OH)_3$, mice received either i.m. and s.c injections (in the right and left thigh respectively), or an i.v. (tail vein) injection of 5 MBq [^{18}F]-fluoride labelled particles (1 mg ml^{-1}) in saline (50 μl). With the mouse under isofluorane anaesthesia in a Minerve imaging chamber, PET/CT scans were acquired from 30 min to 4 h post-injection (p.i.) using a NanoPET/CT scanner (Bioscan, Paris, France) with PET acquisition time 1,800 s, coincidence relation: 1–3; image reconstruction: ordered subset expectation maximisation (OSEM) with single-slice rebinning (SSRB) 2-D line of response (LOR), energy window: 400–600 keV, filter: Ram-Lak cut-off 1, number of iterations/subsets: 8/6. Animals were culled at 4 h p.i. and tissues explanted, blotted dry, weighed and counted on a gamma counter (the carcass activity was measured with an ionisation chamber cross-calibrated with the gamma counter).

Results

Characterisation of particles

Three different samples (HA2, HA3, HA4) have been synthesised and compared to the commercially available hydroxyapatite NPs (HA1). Differences in the experimental protocol led to a variation of both the size and the shape of the particles (see Table 2). Aggregates of almost spherical nanocrystals (HA2), rod-like (HA3) or needle-like (HA4) NPs were obtained (Fig. 1). Characterisation of the different samples confirmed that hydroxyapatite had been obtained whatever the experimental conditions. Indeed, all the XRD diffractograms were identical to that of commercial sample (HA1) and conformed to the ICSD-22059 reference (ESI). Moreover, the FT-IR spectra of the all the samples exhibited bands characteristic of hydroxyapatite due to PO_4^{3-} ions at 1092 cm^{-1}, 1030 cm^{-1}, 963 cm^{-1}, 603 cm^{-1} and 563 cm^{-1}. Additional bands at 1737 cm^{-1} and 1366 cm^{-1} corresponding to CO_3^{2-} were also observed on sample HA2 and can be related to carbon dioxide insertion during sintering of the NPs under air.[37] The thermally treated samples (HA2 and HA3) have a smaller size and narrower size dispersion than HA1 (see Table 2 and Fig. 1). In the case of HA4, the mild conditions of pressure and temperature led to thin needles. Zeta potential measurements on samples HA1, HA2 and HA3 indicated that the particles were negatively charged (−10.7 ± 0.6, −15.8 ± 0.2 and −6.0 ± 0.6 mV respectively). This was not sufficient to prevent aggregation of the NPs in solution, as demonstrated by the DLS measurements. Moreover, despite the use of surfactants (HA4), aggregates were still observable on TEM images. In order to reduce the interactions between the particles, functionalisation with a ligand bearing a stronger anchoring group than the ammonium moiety of the CTAB molecules was used. Two sets of samples (HA4-Ale and HA4-PEG) were synthesised using bisphosphonate (Alendronate) or carboxyl-terminated polyethylene glycol (MeO-PEG-COOH). These ligands are likely to bind to the calcium ions at the surface of the HA NPs *via* the phosphonate or the carboxyl groups respectively. The least aggregation was obtained for the pegylated sample HA4-PEG (see *in vivo* experiments in the next section). It has been reported that the Alendronate can have two different grafting modes due to the phosphonate and amine functional groups and might thus act as a linker between the particles.[38] Infrared analysis after washing of the HA4-PEG particles confirms

the grafting of the PEG (2887 cm^{-1}, 1735 cm^{-1}, 1342 cm^{-1} and 842 cm^{-1} in addition to bands originating from the HA4 mineral; see ESI). No change in the size of the particles due to the surface modification was observed by TEM.

The mesoporous silica particles were obtained according to the protocol published by Bein and co-workers.[36] After synthesis of the NPs the organic template (CTAC) entrapped inside the pores was removed by acid washing, while monitoring by FT-IR (ESI). These NPs were mainly spherical but the formation of larger particles due to the coupling of the smaller ones was also observed, in agreement with earlier work.[36] The pores can be clearly seen on the TEM images (not shown). The XRD diffractogram (ESI) only exhibits one broad peak centered at 22° confirming that the material is amorphous or of insufficient density for the diffraction of the X-rays.

The aluminium hydroxide ($Al(OH)_3$, Alhydrogel™) suspension was used as received. Dilutions in deionised water were made to allow the use of concentrations from 0.1 to 1 mg mL^{-1}. The suspension was characterised using DLS giving a size of 1211 ± 64 nm in agreement with the value reported by the manufacturer.[39]

Initial screening for [^{18}F]-fluoride binding

Preliminary binding studies using hydroxyapatite (HA1, HA2 and HA3) with [^{18}F]-fluoride in water established that binding equilibrium was generally reached well within 5 min even with samples containing less than 1 mg particles in 1 ml suspension. Prolonged incubation for up to 60 min did not increase the percent of radioactivity associated with the NPs. Similar conditions (5 min incubation in water with particles suspended at 1 mg ml^{-1}) were therefore adopted for all subsequent screening. The materials in Table 1 were chosen based on the expected behaviour of fluoride ions taking into account their known preference for binding to hard metal ions, with additional materials included for comparison and contrast. Iron oxide was of interest because of its use as a MR contrast agent material, and silica because of its ubiquitous application as a basis for nanoparticles for biological application. Results of the initial survey are shown in Fig. 2.

Hydroxyapatite showed very high % binding while surprisingly, other related calcium salts did not. Aluminium hydroxide also showed very high % binding. Magnesium oxide, aluminium and erbium oxide showed a high affinity for fluoride under these conditions, while zirconium oxide showed relatively low affinity despite the well-known affinity of soluble zirconium complexes for fluoride.[3] The binding efficiency of aluminium (particles of which are expected to have an aluminium oxide surface) was remarkably high considering its particle size is greater, and therefore its surface area lower, than the equivalent mass of the other nanoparticles. Based on these initial results, hydroxyapatite and aluminium hydroxide particles, which not only showed the highest binding but are highly biocompatible, were selected for further evaluation as fluoride binding materials with a view towards *in vivo* use.

The effect of the method of preparation and surface derivatisation was determined for a range of hydroxyapatite NPs. The method of preparation (untreated, hydrothermal, calcined) made little difference to the labelling efficiency but surface derivatisation with PEG or Alendronate significantly impaired either the rate or extent (it is not possible to determine which with the present data) of fluoride binding, in line with the concentration of the respective ligand used to derivatise the NPs (Fig. 2).

Binding efficiency of [^{18}F]-fluoride to HA and Al(OH)$_3$ in water

To provide an objective measure of fluoride binding affinity allowing semi-quantitative comparison between materials, we adopted particle concentration at half-maximal % binding after 5 min incubation (it is assumed on the basis of the above data that the system is close to equilibrium by this time) of no-carrier-added [^{18}F]-fluoride with suspensions containing different concentrations of particles (HA1, HA2, HA3, Al(OH)$_3$). Examples of the binding curves are shown in Fig. 3 and the data are summarised in Table 3. Efficient binding was observed even at concentrations below 1 mg ml^{-1} in all cases and Al(OH)$_3$ had the highest affinity (lowest K_d). The different methods of preparation of HA had little effect on these parameters.

To study the fluoride loading capacity of these materials, a study was carried out with varying concentrations of *cold* (non-radioactive) fluoride at different particle concentrations (graphs below). The Al(OH)$_3$ particles had markedly higher fluoride binding capacity than hydroxyapatite (HA1) (Fig. 4). Aluminium hydroxide particles showed higher [^{18}F]-fluoride binding than the same concentration (mg ml^{-1}) of hydroxyapatite at all carrier fluoride concentrations used. From these data we estimate that the binding capacity of the HA1 and HA2 particles for fluoride is in the order of 0.1 μmol mg^{-1}. The binding capacity for Al(OH)$_3$ was approximately 10 μmol fluoride/mg NPs and about two orders of magnitude higher than that of HA NPs. The relatively high capacity of the Al(OH)$_3$ may be due to its permeable gel-like nature (see TEM images in ESI). At these levels of affinity and capacity, it is clear that for both HA and Al(OH)$_3$ NPs, at quantities of NPs (*e.g.* $\gg$ 0.1 mg) likely to be used *in vivo* no-carrier-added fluoride binding to nanoparticles will not be limited by saturation or competition from background levels of ^{19}F fluoride ions.

Binding of [^{18}F]-fluoride to HA and Al(OH)$_3$ in the presence of competitors

The modification and application of the particles *in vivo* requires the presence of solutes other than water, which may inhibit binding. Therefore the binding of [^{18}F]-fluoride to HA and Al(OH)$_3$ was tested in the presence of several potential competitive inhibitors, which included simple anions (chloride, citrate, phosphate) and other compounds that may be used in the synthesis or derivatisation of HA nanoparticles. These included sodium hexametaphosphate (HMP), cetyltrimethylammonium bromide (CTAB) and the aminobisphosphonate Alendronate. Among the substances tested, HMP and citrate had the most marked effect on fluoride binding; however, surprisingly high concentration of citrate and HMP was required to reduce fluoride binding significantly (see ESI). Chloride, alendronate and CTAB did not show significant inhibition at any of the concentrations employed (up to at least 0.1 M). Likewise phosphate buffered saline and tris buffer had only a modest inhibitory effect. The lack of effect of aminobisphosphonate is remarkable considering that bisphosphonates have very high binding affinity for the surface of hydroxyapatite.[40]

If these materials are to be used *in vivo*, components in the biological milieu may also have competitive or inhibitory effects on fluoride binding. Therefore, we monitored the stability of [^{18}F]-fluoride-labelled particles added to human serum (see below), and the labelling process conducted in human serum. Fluoride binding to hydroxyapatite was markedly slower in human serum than in water, although given time the % binding levels achieved are comparable (Fig. 5). It should be noted that the human serum used in our experiments contains added citrate (10 mM), which is a known competitor for fluoride binding (see ESI). The effect of serum on labelling of Al(OH)$_3$ was more marked and % binding was severely reduced in serum. The tissue culture medium used in the macrophage experiments had similar effects.

Two serum proteins were tested to determine whether they could play a part in this inhibition of binding: fetuin, because it is known to bind strongly to calcium salts, and albumin because of its high concentration in blood. Neither protein caused a significant reduction in binding (although it should be noted that the concentration of each protein used in the experiment was about 10-fold lower than physiological). In the presence of both albumin and fetuin simultaneously, each at about half the physiological concentration, there was likewise no significant reduction in ^{18}F binding.

Kinetic stability of [^{18}F]-labelled HA and Al(OH)$_3$

For the radiolabelled materials to be used *in vivo* in molecular imaging, the NP-fluoride bond must resist major dissociation in biological media for a period compatible with imaging. Repeated washing of labelled HA and Al(OH)$_3$ with water did not remove a significant fraction of the radioactivity, and even incubation with high concentrations of bisphosphonates (Alendronate, known to have very high affinity for hydroxyapatite) failed to release significant radiolabel over a 2 h period. Incubation of HA in human serum also resulted in minimal radiolabel loss over a period of at least 2 h. However, radiolabelled Al(OH)$_3$ lost radiolabel steadily to the extent of about 50% by 30 min when incubated in serum; this may have been accelerated by dissolution of the particles due to the presence of citrate in the serum.

In vitro cell studies

One of the key features of the *in vivo* behaviour of nanoparticulate materials is clearance by the reticulendothelial system in which phagocytic cells — macrophages, Kupffer cells *etc.* — are the main players. In some applications this is an advantage while in others it must be protected against. We have therefore studied the interaction or the hydroxyapatite and Al(OH)$_3$ particles with cultured macrophages (J774.1) *in vitro* using a combination of radiolabelling and electron microscopy. [^{18}F]-labelled HA4 and Al(OH)$_3$, and [^{18}F]-fluoride as a control, were incubated with J774.1 cells. [^{18}F]-fluoride alone was not significantly taken up by macrophages (<0.2%), whereas the [^{18}F]-fluoride-labelled HA showed progressive association with cells reaching over 70% uptake by 3 h (Fig. 7). Uptake of labelled Al(OH)$_3$ was much less marked during this period, although given the more rapid release of radioactivity from these particles (Fig. 6) it is possible that there is rapid uptake followed by rapid release of free fluoride. The phagocytic uptake of HA and Al(OH)$_3$ particles was confirmed by electron microscopy (Fig. 7) which showed the presence of aggregates of particles within endosomes in the cytoplasm of the cells.

In vivo studies

The observation that the association of [^{18}F]-fluoride with hydroxyapatite particles (and to a lesser extent Al(OH)$_3$) is kinetically stable in a variety of challenging media including human serum shows that the *in vivo* fate of the nanoparticles, and the *in vivo* stability of the radiolabel, can be monitored *in vivo* by PET imaging. The latter is possible because [^{18}F]-fluoride released from nanoparticles *in vivo* would show a distinctive pattern of uptake in the joints of the skeleton. Labelled particles were administered by the sub-cutaneous, intramuscular and intravenous routes. The observed biodistribution of [^{18}F]-labelled hydroxyapatite nanoparticles in normal mice was dependant on the route of administration and the state of aggregation of the particles. PET and PET-CT scans are shown in Fig. 8 and Fig. 9, and biodistribution data are provided in ESI. [^{18}F]-fluoride-labelled HA4 injected by the subcutaneous and intramuscular route remained at the injection site and negligible translocation of radioactivity to other sites was seen during the 4 h study period (see ESI). [^{18}F]-HA2 particles, which are largely aggregated, are trapped by embolisation in the lungs after intravenous injection. A few particles small enough to escape this biological filtration

mechanism are taken up in liver or excreted renally. There is no significant uptake in the joints of the skeleton even after 4 h, indicating that particles trapped thus in the lung capillary bed are stable towards loss of radiolabel. [^{18}F]-HA4 is a less aggregated form of HA and showed correspondingly less lung trapping and more uptake in liver and spleen, consistent with the observed phagocytic uptake shown in Fig. 7. In this instance, over the four hours of the study, radioactivity was gradually released and accumulated in the skeleton (Fig. 8), suggesting that once taken up by the reticuloendothelial system, degradation and release of fluoride takes place. Particles that are further protected from aggregation by PEGylation (HA4-PEG-0.1) show even less trapping in lung and more in liver and spleen at 30 min, which is largely translocated to the joints subsequently.

[^{18}F]-labelled $Al(OH)_3$ particles were injected intramuscularly (right thigh, Fig. 9) and subcutaneously (left thigh) in the same animal. Almost all radioactivity remained at the sites of injection during the entire scanning period of 4 h. There was evidence of only slight translocation of radioactivity to the joints by 4 h, indicating that the radiolabelled particles are moderately stable *in vivo* over this time period. When the particles were injected intravenously, there was no lung trapping and radioactivity was cleared from blood rapidly by uptake in the liver and spleen and by renal excretion. Translocation of the liver and spleen activity to the joints was faster than for i.v. injected HA and faster than for s.c. and i.m. injected $Al(OH)_3$, suggesting that the degradation and release of soluble radioactivity occurs in mainly liver and spleen. The large amount of radioactivity appearing rapidly in the bladder suggests that the particles may be broken down into soluble fragments small enough for renal filtration, but not releasing free fluoride since uptake in the joints is low at the 30 min scan. Extensive joint uptake, suggesting release of free fluoride, occurs later than the renal excretion.

Discussion and conclusions

The design of molecular imaging contrast agents based on nano-particulate carriers requires several contributing components: the nanoparticle itself, a means of derivatising it in a stable manner to control its biodistribution (for prevention of aggregation, control of reticuloendothelial clearance and molecular targeting), and a means of attaching the imaging probe (gamma or positron emitting radionuclide, gadolinium contrast agent, fluorescent tag, *etc.*). At the present early stage of development of this field, the nanoparticles reported so far have been chosen from a very restricted range of materials-typically silica and gold nanoparticles, cadmium-based quantum dots, and superparamagnetic iron oxide nanoparticles. In this work we have begun to extend the choice of nanoparticulate material with the aim of developing systems that are amenable to use with PET imaging whilst minimising the complexity of the radiochemical synthesis required. By selecting [^{18}F]-fluoride as the radiolabel, we reduce the radiochemistry to the simplest level possible. This introduces a requirement for a nanoparticulate material that can be quickly and efficiently labelled with [^{18}F]-fluoride in mild aqueous conditions and without need for complex purification steps. We screened a number of likely inorganic materials for this property, at the same time keeping in mind the need for a high degree of biocompatibility and low toxicity. Two materials emerged satisfying both requirements: hydroxyapatite and aluminium hydroxide. The factors affecting the binding of fluoride to these particles and the stability of the bond once formed were studied under biological conditions. The radiolabelling of hydroxyapatite proved to be robust, resistant to a variety of potential inhibitors, and adequate for *in vivo* imaging applications. The particles are prone to aggregation but this can be minimised by surface modification with alendronate or PEG while still retaining adequate capacity for radiolabelling. The labelling is stable *in vivo* unless the particles are taken up by the reticuloendothelial system, whereupon degradation and release of fluoride takes place over a period of several hours. It has been shown

previously that hydroxyapatite particles are readily surface-modified by bisphosphonates (as seen in this case with alendronate), providing a means of attaching targeting functionality or other radionuclides using bisphosphonate conjugates of radionuclides,[40,41] proteins and peptides (unpublished work). We have also shown here that they can be readily radiolabelled simply by brief incubation with [^{18}F]-fluoride in aqueous media, and that the radiolabel has adequate stability for *in vivo* imaging. Hydroxyapatite nanoparticles represent a promising basis for assembly of targeted PET molecular imaging agents for labelling with [^{18}F]-fluoride. Aluminium hydroxide gel nanoparticles share the property of highly efficient and convenient radiolabelling with [^{18}F]-fluoride, and they too are highly biocompatible (the particles used here are commercially available for use as adjuvants in vaccines). They also have an extraordinary capacity to sequester a high payload of fluoride per nanoparticle. Fluoride is known to be capable of occupying the hydroxide sites in hydroxyapatite[42] and we speculate that hydroxide ions may be displaced by fluoride at the crystal surface; alternatively or additionally hydrogen fluoride may be bound by hydrogen bonding or dipolar bonds at the crystal surface, since the experimental conditions are not basic. Similarly, in aluminium hydroxide, fluoride may be bound directly to aluminium ions by displacement of hydroxide, given its known ability to coordinate strongly to aluminium ions.[6,7] However, they are subject to more rapid degradation in the biological milieu than hydroxyapatite, and this degradation needs to be curtailed by further modification before use in imaging applications, except for very short time scale studies. Because of the simplicity of the radiolabelling, which eliminates the need for costly robotics for complex automated synthesis which often limits the wider application of ^{18}F-labelled radiopharmaceuticals, both hydroxyapatite and aluminium hydroxide provide a promising basis for development of biocompatible, low-toxicity nanoparticulate contrast agents for multimodality molecular imaging *in vivo*. Further work is required to develop approaches to modify the surface to attach a range of biological targeting molecules, modifying aggregation, reticulendothelial uptake and providing molecular targeting. For molecular targeting purposes, hydroxyapatite nanoparticles can be surface-modified with bisphosphonate bioconjugates of peptides and proteins; synthesis of such bioconjugates will be described in future publications.

Supplementary Material

Refer to Web version on PubMed Central for supplementary material.

Acknowledgments

We thank Ms Kelly Rausch (NIH, Bethesda, USA) for providing a sample of Alhydrogel™. This work was funded by the Centre of Excellence in Medical Engineering funded by the Wellcome Trust and EPSRC under grants (WT 088641/Z/09/Z). MJ-O was supported by an EPSRC postdoctoral fellowship at the Life Sciences Interface. PAW was supported by a Harris studentship. We thank the Wellcome Trust for an equipment grant for purchase of the PET-CT scanner.

References

1. Cametti M, Rissanen K. Chem. Commun. 2009:2809.
2. Hudnall TW, Chiu CW, Gabbai FP. Acc. Chem. Res. 2009; 42:388. [PubMed: 19140747]
3. Takahashi Y, Pacheco Tanaka DA, Matsunaga H, Suzuki TM. J. Chem. Soc. Perkin Trans. 2002:759.
4. Schlyer DJ, Bastos MA, Alexoff D, Wolf AP. Int. J. Radiat. Appl. Instrum., Part A. 1990; 41:531.
5. McBride WJ, D'Souza CA, Sharkey RM, Karacay H, Rossi EA, Chang C-H, Goldenberg DM. Bioconjugate Chem. 2010; 21:1331.
6. Laverman P, McBride WJ, Sharkey RM, Eek A, Joosten L, Oyen WJG, Goldenberg DM, Boerman OC. J. Nucl. Med. 2010; 51:454. [PubMed: 20150268]

7. McBride WJ, Sharkey RM, Karacay H, D'Souza CA, Rossi EA, Laverman P, Chang C-H, Boerman OC, Goldenberg DM. J. Nucl. Med. 2009; 50:991. [PubMed: 19443594]
8. Hudnall TW, Lin T-P, Gabbaí FP. J. Fluorine Chem. 2010; 131:1182.
9. Studenov AR, Adam MJ, Wilson JS, Ruth TJ. J. Labelled Compd. Radiopharm. 2005; 48:497.
10. Mu L, Hohne A, Schubiger PA, Ametamey SM, Graham K, Cyr JE, Dinkelborg L, Stellfeld T, Srinivasan A, Voigtmann U, Klar U. Angew. Chem., Int. Ed. 2008; 47:4922.
11. Bohna P, Deyine A, Azzouz R, Bailly L, Fiol-Petit C, Bischoff L, Fruit C, Marsais F, Vera P. Nucl. Med. Biol. 2009; 36:895. [PubMed: 19875046]
12. Schirrmacher R, Bradtmoller G, Schirrmacher E, Thews O, Tillmanns J, Siessmeier T, Buchholz HG, Bartenstein P, Wangler B, Niemeyer CM, Jurkschat K. Angew. Chem., Int. Ed. 2006; 45:6047.
13. Nandy SK, Rajan MGR. J. Radioanal. Nucl. Chem. 2010; 286:241.
14. Jauregui-Osoro M, Sunassee K, Weeks AJ, Berry DJ, Paul RL, Cleij M, Banga J, O'Doherty MJ, Marsden PK, Clarke SEM, Ballinger JR, Szanda I, Cheng SY, Blower PJ. Eur. J. Nucl. Med. Mol. Imaging. 2010; 37:2108. [PubMed: 20577737]
15. Badillo-Almaraz VE, Armando Flores J, Arriola H, López FA, Ruiz-Ramirez L. J. Radioanal. Nucl. Chem. 2007; 271:741.
16. Motskin M, Wright DM, Muller K, Kyle N, Gard TG, Porter AE, Skepper JN. Biomaterials. 2009; 30:3307. [PubMed: 19304317]
17. Volker JF, Carpenter Hodge H, Wilson HJ, van Voorhis SN. J. Biol. Chem. 1940; 134:543.
18. Ho NL, Ishihara T, Ueshima S, Nishiguchi H, Takita Y. J. Colloid Interface Sci. 2004; 272:399. [PubMed: 15028504]
19. Samatya S, Yuksel U, Yuksel M, Kabay N. Sep. Sci. Technol. 2007; 42:2033.
20. Kao HM, Liao YC. J. Phys. Chem. C. 2007; 111:4495.
21. Bassindale AR, Pourny M, Taylor PG, Hursthouse MB, Light ME. Angew. Chem., Int. Ed. 2003; 42:3488.
22. Ting R, Harwig C, auf dem Keller U, McCormick S, Austin P, Overall CM, Adam MJ, Ruth TJ, Perrin DM. J. Am. Chem. Soc. 2008; 130:12045. [PubMed: 18700764]
23. Hammari LEL, Laghzizila A, Barboux P, Lahlil K, Saoiabi A. J. Hazard. Mater. 2004; 114:41. [PubMed: 15511572]
24. Devaraj NK, Keliher EJ, Thurber GM, Nahrendorf M, Weissleder R. Bioconjugate Chem. 2009; 20:397.
25. Welch MJ, Hawker CJ, Wooley KL. J. Nucl. Med. 2009; 50:1743. [PubMed: 19837751]
26. Matson JB, Grubbs RH. J. Am. Chem. Soc. 2008; 130:6731. [PubMed: 18452296]
27. Dormer KJ, Awasthi V, Galbraith W, Kopke RD, Chen K, Wassel R. J. Biomed. Nanotechnol. 2008; 4:174.
28. Jarrett BR, Gustafsson B, Kukis DL, Louie AY. Bioconjugate Chem. 2008; 19:1496.
29. Le Bars D. J. Fluorine Chem. 2006; 127:1488.
30. Aimanianda V, Haensler J, Lacroix-Desmazes S, Kaveri SV, Bayry J. Trends Pharmacol. Sci. 2009; 30:287. [PubMed: 19439372]
31. Hem SL, HogenEsch H. Expert Rev. Vaccines. 2007; 6:685. [PubMed: 17931150]
32. Jiang D, Premachandra GS, Johnston C, Hem SL. Vaccine. 2004; 23:693. [PubMed: 15542192]
33. Xing ZC, Chang YM, Kang IK. Sci. Tech. Advanced Mater. 2010; 11:1.
34. Burns A, Sengupta P, Zedayko T, Baird B, Wiesner U. Small. 2006; 2:723. [PubMed: 17193111]
35. US Pat., 7411087. 2008.
36. Möller K, Kobler J, Bein T. Adv. Funct. Mater. 2007; 17:605.
37. Slosarczyk A, Paszkiewicz Z, Paluszkiewicz C. J. Mol. Struct. 2005; 744-747:657.
38. Mukherjee S, Huang CC, Guerra F, Wang K, Oldfield E. J. Am. Chem. Soc. 2009; 131:8374. [PubMed: 19489581]
39. Lindblad EB. Immunol. Cell Biol. 2004; 82:497. [PubMed: 15479435]

40. Torres R, Martin de Rosales, Finucane C, Foster J, Mather SJ, Blower PJ. Bioconjugate Chem. 2010; 21:811.
41. de Rosales RTM, Finucane C, Mather SJ, Blower PJ. Chem. Commun. 2009:4847.
42. de Leeuw NH. J. Mater. Chem. 2010; 20:5376.

Europe PMC Funders Author Manuscripts

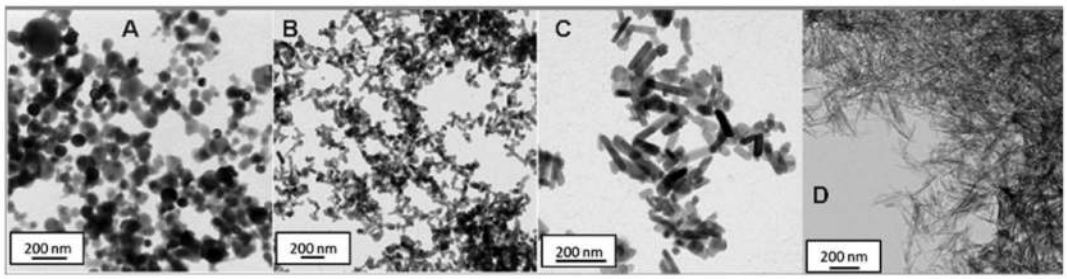

Fig. 1.
Transmission electron micrographs of hydroxyapatite used in this study: A) commercially available (HA1); B) calcined (HA2); C) hydrothermally treated (HA3); D) without any thermal treatment (HA4).

Europe PMC Funders Author Manuscripts

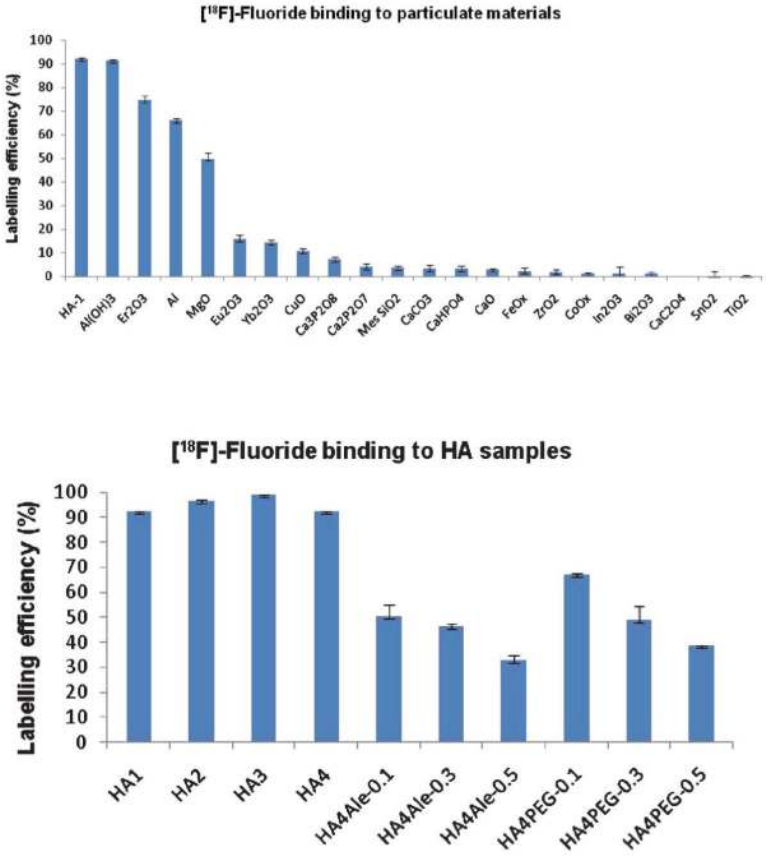

Fig. 2.

Top: Initial screening of various inorganic materials for [^{18}F]-fluoride binding. Bottom: comparison of [^{18}F]-fluoride binding efficiency of hydroxyapatite nanoparticles prepared by different methods (HA1: commercial; HA2: calcined; HA3: hydrothermal; HA4: no treatment) including increasing surface modification with Alendronate (HA4Ale) and PEG (HA4PEG). The charts show labelling efficiency (percent bound radioactivity) after incubation of [^{18}F]-fluoride solution (100 μL, 6 MBq) with a 1 mg ml^{-1} suspension of the particles in water (1 ml) at room temperature for 5 min.

Europe PMC Funders Author Manuscripts

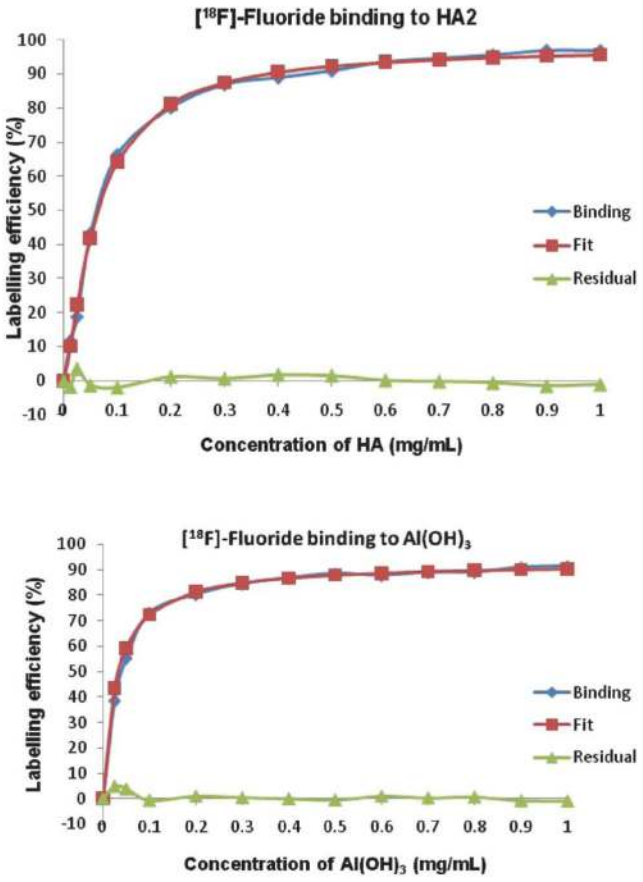

Fig. 3.

Binding efficiency of no-carrier-added [^{18}F]-fluoride to hydroxyapatite HA2 (top) and $Al(OH)_3$ (bottom) as a function of nanoparticle concentration. Chart shows labelling efficiency (percent bound radioactivity) after incubation of [^{18}F]-fluoride solution (100 μL, 6 MBq) with a suspension of HA in water (1 ml) at room temperature for 5 min.

Europe PMC Funders Author Manuscripts

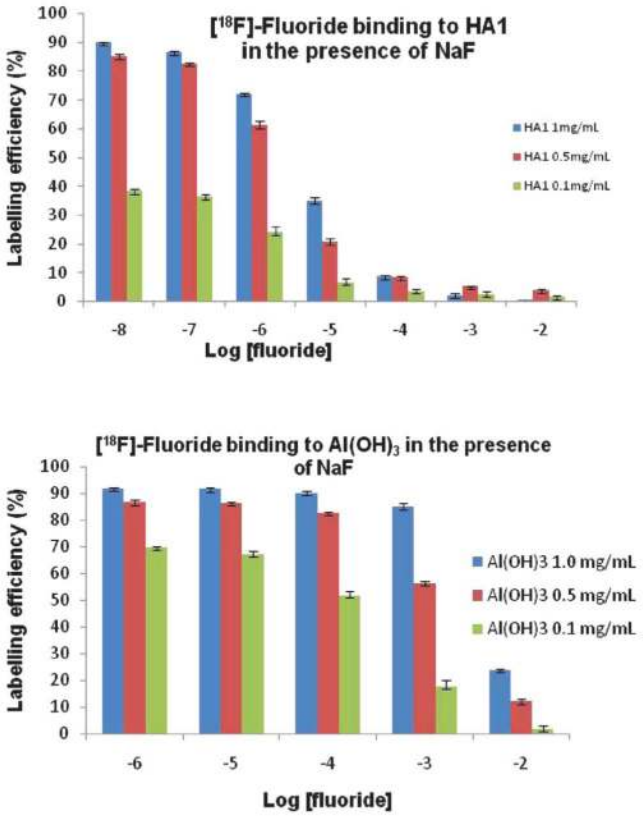

Fig. 4.

Effect of carrier fluoride concentration on binding of [^{18}F]-fluoride to HA1 (top) and $Al(OH)_3$ (bottom) particles. [^{18}F]-fluoride solution (100 μL, 6 MBq) was incubated with a suspension of particles (1.0, 0.5 and 0.1 mg ml^{-1}) in aqueous solutions (1 ml) of sodium fluoride of varying concentrations at room temperature for 5 min. Corresponding data for HA2 can be found in ESI.

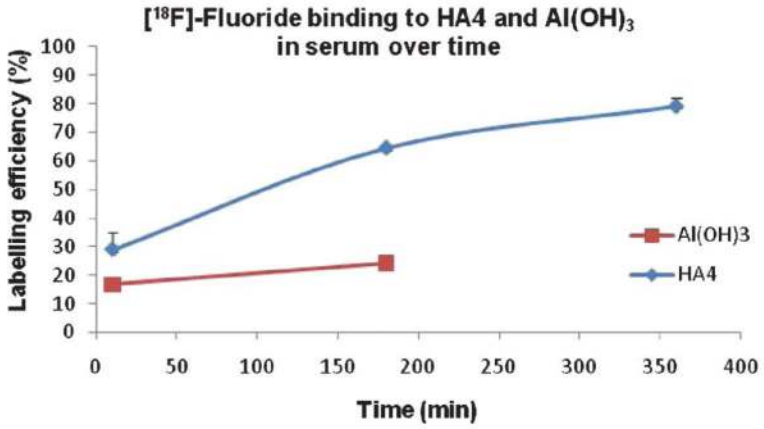

Fig. 5.

[^{18}F]-fluoride binding of HA4 and $Al(OH)_3$ in serum as a function of incubation time. [^{18}F]-fluoride (100 μl) was incubated with a suspension of particles (0.5 mg ml^{-1}) in human serum (1 ml) at 37 °C with continuous shaking for 6 h. Binding is delayed compared to labelling in water, which is complete within 5 min.

Europe PMC Funders Author Manuscripts

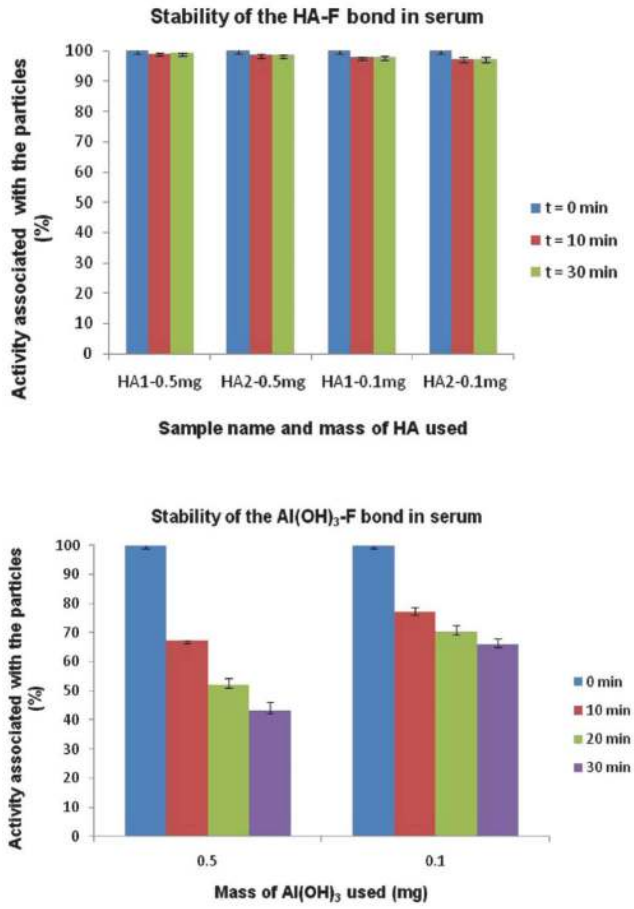

Fig. 6.

Rate of loss of radiolabel from [^{18}F]-fluoride-labelled HA (top) and $Al(OH)_3$ (bottom) particles during incubation in serum. Charts show % activity remaining associated with pre-labelled, washed particles after incubation, with initial activity defined as 100%.

Europe PMC Funders Author Manuscripts

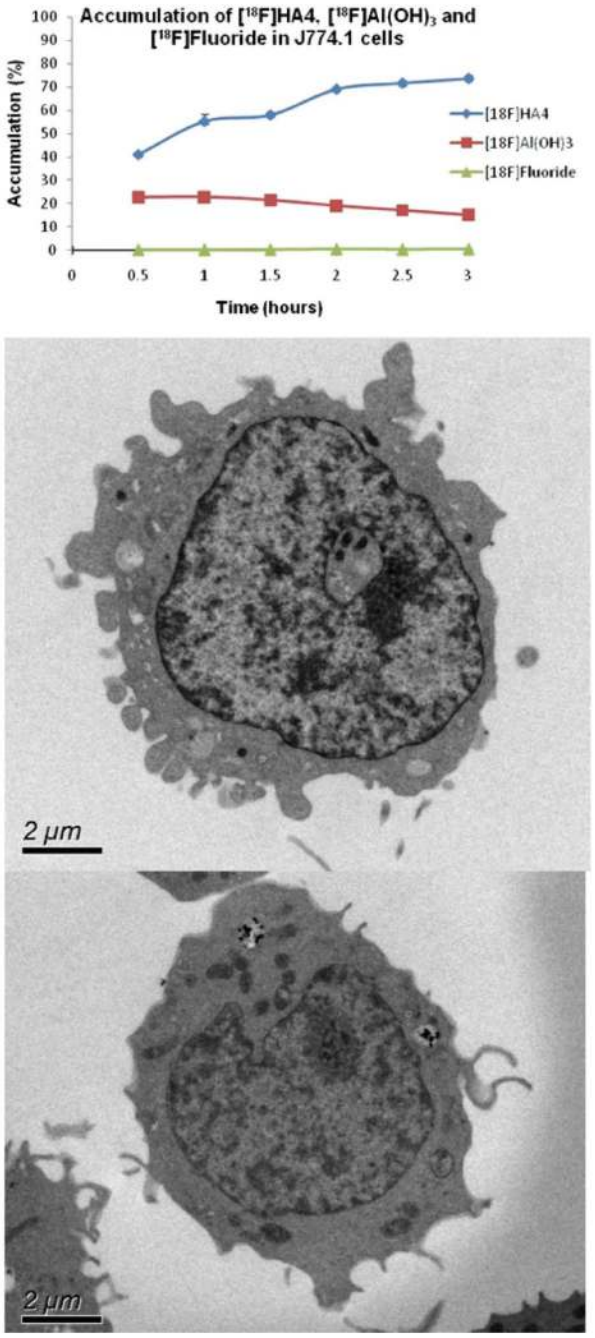

Fig. 7.

Uptake of [^{18}F]-HA4, [^{18}F]-Al(OH)$_3$ and [^{18}F]-fluoride (control) in macrophages (top), and transmission electron micrographs of macrophages before (centre) and after (bottom) incubation with HA1, showing HA1 particles sequestered within phagosomes in the macrophages (bottom). Corresponding images showing Al(OH)$_3$ uptake are shown in ESI.

Europe PMC Funders Author Manuscripts

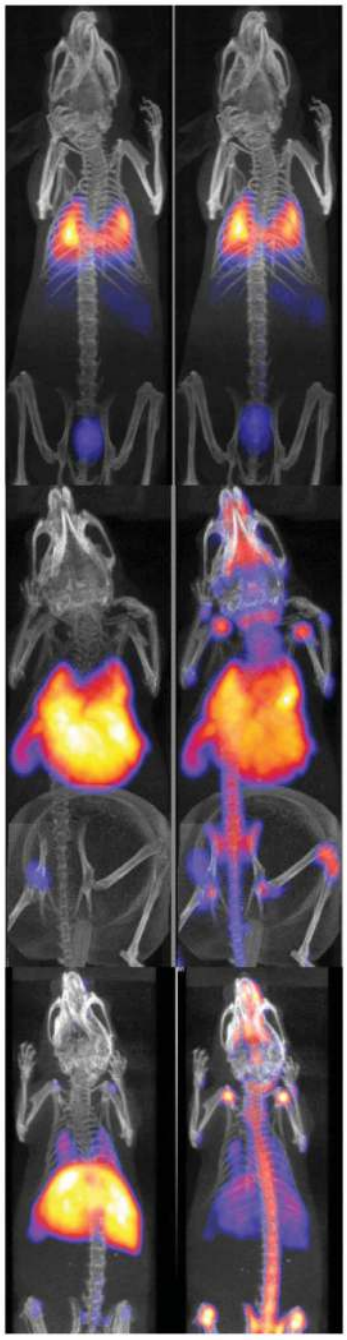

Fig. 8.

PET-CT scans (maximum intensity projection) of mice after i.v. injection of [^{18}F]-fluoride labelled hydroxyapatite, at 30 min (left) and 4 h (right) post injection. Top: [^{18}F]-labelled HA2 (highly aggregated); Middle: HA4 (moderately aggregated); Bottom: PEG-modified HA4-PEG-0.1. There is a trend towards less lung uptake and more liver and spleen uptake as aggregation is reduced. Higher liver and spleen uptake is associated with more pronounced transfer of radioactivity to the joints with time.

Europe PMC Funders Author Manuscripts

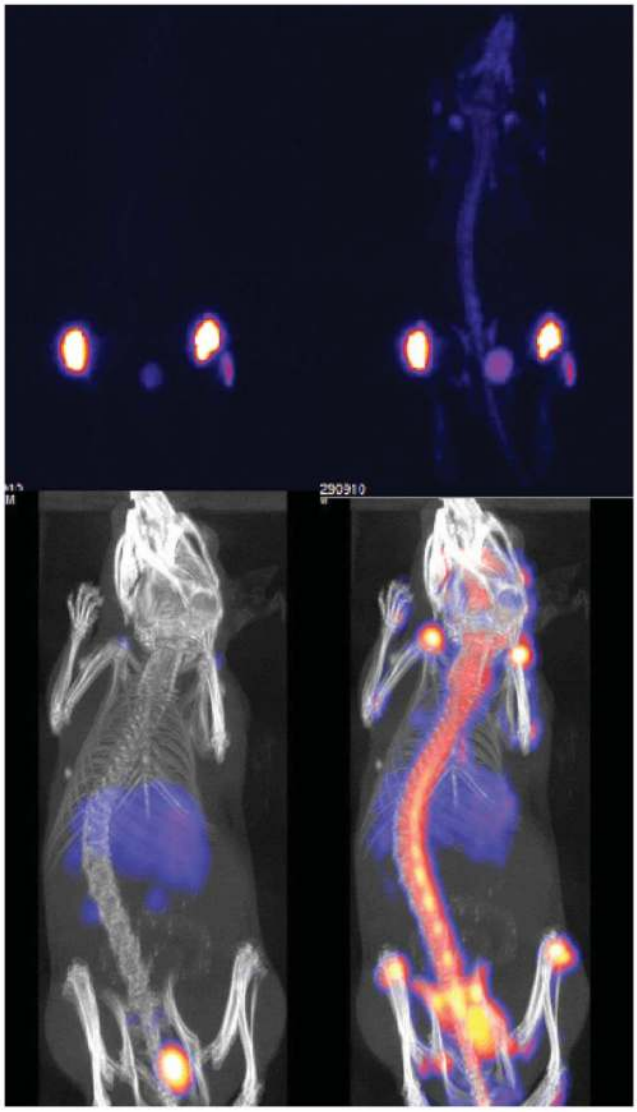

Fig. 9.

PET and PET-CT scans of mice 30 min (left) and 4 h (right) post injection of [^{18}F]-fluoride-labelled $Al(OH)_3$. Top: after intramuscular (right thigh) and subcutaneous (left thigh) injection (CT scan omitted in order to reveal skeletal uptake more clearly); Bottom: after intravenous injection. Intramuscular and subcutaneous administrations led to minimal translocation of radioactivity from the injection site and to the joints, whereas intravenous injection led to early uptake in liver, spleen and bladder with later translocation from liver and spleen to the joints.

Europe PMC Funders Author Manuscripts

Table 1

Particulate materials used in this study, their origin and size (stated by the manufacturer except [a]size and standard deviation measured by dynamic light scattering, with standard deviation)

Material	Origin	Size
$Al(OH)_3$-Alhydrogel™	Brenntag Biosector (Frederikssund, Denmark)	1211 ± 64 nm[a]
Al	Sigma–Aldrich	< 75 μm
Ag	Sigma–Aldrich	<100 nm
Bi_2O_3	Sigma–Aldrich	90–210 nm
CaO	Sigma–Aldrich	<160 nm
$[Ca_5(OH)(PO_4)_3]_x$ – HA1	Sigma–Aldrich	<200 nm
Co_3O_4	Sigma–Aldrich	<50 nm
CuO	Sigma–Aldrich	<50 nm
Er_2O_3	Sigma–Aldrich	<100 nm
Eu_2O_3	Sigma–Aldrich	<150 nm
Fe_3O_4	Sigma–Aldrich	<50 nm
In_2O_3	Sigma–Aldrich	<100 nm
MgO	Sigma–Aldrich	<50 nm
SnO_2	Sigma–Aldrich	<100 nm
TiO_2	Sigma–Aldrich	<100 nm
Yb_2O_3	Sigma–Aldrich	<100 nm
ZrO_2	Sigma–Aldrich	<100 nm

Europe PMC Funders Author Manuscripts

Table 2

Hydroxyapatite and silica nanoparticles synthesised in this work. Size and standard deviation was measured by transmission electron microscopy (TEM) and dynamic light scattering (DLS)

Designation	Post-synthesis treatment	Size by TEM (nm)	Size by DLS (nm)
Mes-SiO_2	none	70.9 ± 8.6	—
HA2	calcination	41.6 ± 1.8	2784 ± 158
HA3	hydrothermal	107.5 ± 6.2 × 25.8 ± 0.9	829 ± 135
HA4	none	132.0 ± 30.3 × 12.6 ± 2.2	2046 ± 470 (main peak)
HA4Ale-0.1	Alendronate, 0.1 ml		169 ± 33 (main peak)
HA4Ale-0.3	Alendronate, 0.3 ml		
HA4Ale-0.5	Alendronate, 0.5 ml	132.0 ± 30.3 × 12.6 ± 2.2	
HA4PEG-0.1	MeO-PEG-COOH, 0.1 ml		214 ± 68
HA4PEG-0.3	MeO-PEG-COOH, 0.3 ml		
HA4PEG-0.5	MeO-PEG-COOH, 0.5 ml		

Europe PMC Funders Author Manuscripts

Table 3

Binding characteristics of HA and $Al(OH)_3$ nanoparticles for binding to [^{18}F]-fluoride. K_d is the nanoparticle concentration at half-maximal % binding; B_{max} is the maximal % binding. $Al(OH)_3$ has the highest effective affinity as indicated by the low K_d value

Material	B_{max} (%)	K_d (mg mL^{-1})	n	r^2
HA2	97.90	0.062	1.35	0.9980
HA1	86.46	0.075	1.65	0.9728
HA3	97.77	0.075	1.92	0.9961
$Al(OH)_3$	92.96	0.028	1.00	0.9986